THE JOURNAL OF BIOLOGICAL CHEMISTRY VOL. 289, NO. 33, pp. 23256–23263, August 15, 2014

The α-Subunit Regulates Stability of the Metal Ion at the Ligand-associated Metal Ion-binding Site in β_3 Integrins*

Received for publication, May 13, 2014, and in revised form, June 23, 2014 Published, JBC Papers in Press, June 28, 2014, DOI 10.1074/jbc.M114.581470

Xianliang Rui[‡1], Mehrdad Mehrbod[§1], Johannes F. Van Agthoven[¶], Saurabh Anand[‡], Jian-Ping Xiong[¶], Mohammad R. K. Mofrad[§2], and M. Amin Arnaout[‡¶3]

From the [‡]Leukocyte Biology and Inflammation Program and [¶]Structural Biology Program, Department of Medicine, Massachusetts General Hospital and Harvard Medical School, Charlestown, Massachusetts 02129 and the [§]Departments of Bioengineering and Mechanical Engineering, University of California, Berkeley, California 94720

Background: Metal ions at LIMBS and MIDAS are essential for integrin-ligand interactions.
Results: MD simulations showed strikingly different and functionally relevant conformations of LIMBS in $\alpha_V\beta_3$ and $\alpha_{IIb}\beta_3$.
Conclusion: The α-subunit regulates metal ion coordination at LIMBS and hence function of β_3 integrins.
Significance: The results reveal a new mechanism of integrin regulation by the α-subunit.

The aspartate in the prototypical integrin-binding motif Arg-Gly-Asp binds the integrin βA domain of the β-subunit through a divalent cation at the metal ion-dependent adhesion site (MIDAS). An auxiliary metal ion at a ligand-associated metal ion-binding site (LIMBS) stabilizes the metal ion at MIDAS. LIMBS contacts distinct residues in the α-subunits of the two β_3 integrins $\alpha_{IIb}\beta_3$ and $\alpha_V\beta_3$, but a potential role of this interaction on stability of the metal ion at LIMBS in β_3 integrins has not been explored. Equilibrium molecular dynamics simulations of fully hydrated β_3 integrin ectodomains revealed strikingly different conformations of LIMBS in unliganded $\alpha_{IIb}\beta_3$ *versus* $\alpha_V\beta_3$, the result of stronger interactions of LIMBS with α_V, which reduce stability of the LIMBS metal ion in $\alpha_V\beta_3$. Replacing the α_{IIb}-LIMBS interface residue Phe^{191} in α_{IIb} (equivalent to Trp^{179} in α_V) with Trp strengthened this interface and destabilized the metal ion at LIMBS in $\alpha_{IIb}\beta_3$; a Trp^{179} to Phe mutation in α_V produced the opposite but weaker effect. Consistently, an F191/W substitution in cellular $\alpha_{IIb}\beta_3$ and a W179/F substitution in $\alpha_V\beta_3$ reduced and increased, respectively, the apparent affinity of Mn^{2+} to the integrin. These findings offer an explanation for the variable occupancy of the metal ion at LIMBS in $\alpha_V\beta_3$ structures in the absence of ligand and provide new insights into the mechanisms of integrin regulation.

Integrins are αβ heterodimeric cell adhesion receptors that mediate divalent cation-dependent cell-matrix and cell-cell adhesion during morphogenesis, as well as the maintenance of tissues and organs in adult life. 18 α- and 8 β-subunits assemble into 24 integrin receptors in mammals. Integrins regulate fundamental aspects of cell behavior, including migration, adhesion, differentiation, growth, and survival, by communicating bidirectional signals between the extracellular environment and the intracellular cytoskeleton (1).

Integrins are unusual receptors as they do not engage physiologic ligand unless activated. This property allows patrolling blood leukocytes and platelets, for example, to circulate without aggregating or interacting with the vessel walls. Inappropriate activation of integrins contributes to the pathogenesis of common diseases including heart attacks, stroke, and cancer growth and metastasis. Thus understanding how these receptors are regulated is important in promoting health and treating disease (2).

The integrin heterodimer comprises a head segment that sits on top of two leg segments each spanning the plasma membrane once and ending with a short cytoplasmic tail. The ligand-binding head consists of a seven-bladed β-propeller domain from the α-subunit that associates noncovalently with a GTPase-like domain, βA, from the β-subunit (3). Contacts between the cytoplasmic tails and transmembrane segments hold the integrin in an inactive state (unable to bind physiologic ligand). Binding of talin to the β-cytoplasmic tail breaks these contacts, switching the ectodomain into the active (ligand-competent) conformation, a process called "inside-out" signaling (4). Ligand binding then triggers global conformational changes that propagate through the plasma membrane to the cytoplasmic tails, leading to "outside-in" signaling.

Integrin-ligand interactions are regulated in a complex manner by divalent cations (5–8). Although Mn^{2+} and, to a lesser extent, Mg^{2+} stimulate ligand binding, Ca^{2+} is typically inhibitory. The ligand-binding face of the βA domain is decorated by three metal ion-binding sites: a metal ion-dependent adhesion site (MIDAS),[4] flanked on one side (facing the propeller domain of the α-subunit) by a ligand-associated metal ion-binding site (LIMBS), and on the opposite side by an Adjacent to MIDAS (ADMIDAS) (9). A ligand aspartate completes the octahedral metal coordination of an Mg^{2+} (or Mn^{2+}) at MIDAS in ligand-

* This work was supported, in whole or in part, by National Institutes of Health Grants DK088327, DK096334, and DK007540 (to M. A. A.) and by a National Science Foundation CAREER Award CBET-0955291 (to M. R. K. M.).
[1] Both authors contributed equally to this work.
[2] To whom correspondence may be addressed: 208A Stanley Hall #1762, University of California, Berkeley, CA 94720. Tel.: 510-643-8165; E-mail: mofrad@berkeley.edu.
[3] To whom correspondence may be addressed: Massachusetts General Hospital, 149 13th St., Charlestown, MA 02129. Tel.: 617-726-5663; E-mail: aarnaout1@mgh.harvard.edu.

[4] The abbreviations used are: MIDAS, metal ion-dependent adhesion site; LIMBS, ligand-associated metal-binding site; ADMIDAS, adjacent to MIDAS; FB, fibrinogen; MD, molecular dynamics; r.m.s.d., root mean square deviation; HBSS, Hank's balanced saline solution.

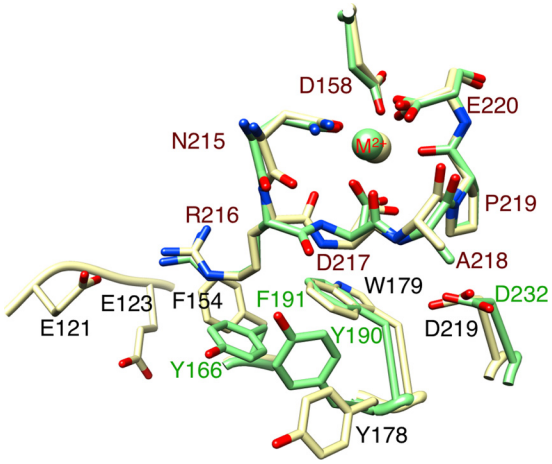

FIGURE 1. **α-subunit residues facing LIMBS in β_3 integrins.** A ribbon diagram showing the residues from α_{IIb} and α_V facing LIMBS loop residues Arg^{216}-Ala^{218} is presented. The β_3 subunits of unliganded $\alpha_{IIb}\beta_3$ (*green*, 3fcs.pdb) and $\alpha_V\beta_3$ (*yellow*, 4g1e.pdb) ectodomains were superposed with Chimera. The metal ion (M^{2+}) at LIMBS (*sphere*) has the color of the respective integrin. α_{IIb} and α_V residues are labeled in *green* and *black*, respectively, and the LIMBS residues are labeled in *red*.

bound integrins. Ca^{2+} but not Mg^{2+} binds preferentially at LIMBS and ADMIDAS in physiologic buffer conditions, and both sites can coordinate Mn^{2+}. The metal ion at LIMBS stabilizes the one at MIDAS (9–11), thus acting as a positive regulator of ligand binding to integrins, whereas the ADMIDAS metal ion can stabilize alternate inactive and active conformations of the integrin (2).

At the ligand-binding face of βA domain, the LIMBS loop residues Arg^{216}, Asp^{217}, and Ala^{218} contact residues in the α-subunit propeller domain (Fig. 1), but a potential role of the α-subunit in regulating metal ion occupancy in the βA domain has not been explored. In this study, we carried out computational and functional studies on the two β_3 integrins $\alpha_V\beta_3$ and $\alpha_{IIb}\beta_3$. Our studies reveal an important role of the α-subunit in regulating metal ion stability at LIMBS in β_3 integrins. The significance of this finding is discussed.

EXPERIMENTAL PROCEDURES

Molecular Dynamics Simulations Design—The crystal structures of the ectodomains of $\alpha_{IIb}\beta_3$ (Protein Data Bank (PDB) 3fcs) (12) and $\alpha_V\beta_3$ (PDB 4g1e) (13) were downloaded from the Protein Data Bank. In $\alpha_{IIb}\beta_3$, LIMBS (also known as SymBS, synergistic metal-binding site), MIDAS, and ADMIDAS were occupied by Ca^{2+}, Mg^{2+}, and Ca^{2+} respectively. Because only LIMBS was metal-occupied (by Ca^{2+}) in unliganded $\alpha_V\beta_3$ structure, Mg^{2+} and Ca^{2+} were respectively placed at MIDAS and ADMIDAS such that their initial distances (*i.e.* before minimization) from all the proximal oxygen atoms were between 2.4 and 4 Å. Mutations were made to the native structures using the software Swiss-Pdb Viewer 4.1.0 (14). All non-protein atoms were removed from $\alpha_{IIb}\beta_3$ and $\alpha_V\beta_3$ structures, leaving α- and β-subunits with nearly 24,000 atoms for each, including hydrogens. Proteins were solvated in water boxes of sizes 168 × 169 × 207 Å (for $\alpha_V\beta_3$) and 180 × 144 × 226 Å (for $\alpha_{IIb}\beta_3$), adding ~183,000 and 185,000 water molecules to $\alpha_V\beta_3$ and $\alpha_{IIb}\beta_3$, respectively, and ionized with 150 mM KCl. To investigate the effects of Phe^{191} in α_{IIb} and Trp^{179} in α_V on coordinating divalent cations at LIMBS, six distinct combinations of cation type and mutation for $\alpha_{IIb}\beta_3$ and four for $\alpha_V\beta_3$ were tested. To investigate the effects of each cation arrangement, the $\alpha_{IIb}\beta_3$ and $\alpha_V\beta_3$ structures were equilibrated with LIMBS-MIDAS-ADMIDAS occupancies of Ca^{2+}-Mg^{2+}-Ca^{2+} and Mn^{2+}-Mn^{2+}-Mn^{2+}.

Molecular Dynamics Simulations—MD simulations of the integrin ectodomain were performed with NAMD cvs_20130828 software package (15). The CHARMM27 force field parameter (16) was used to model the protein. The TIP3P model (17) was used for water molecules. Structures were visualized with Visual Molecular Dynamics (VMD) (18) or Chimera (19). The crystal structures of the ligand-free forms of $\alpha_{IIb}\beta_3$ and of $\alpha_V\beta_3$ ectodomains were used without modification, except for the manual placement of metal ions at LIMBS and ADMIDAS in $\alpha_V\beta_3$ and the removal of the sugar and water molecules before solvation. All simulations were carried out at the computing facilities of the National Energy Research Scientific Computing Center (NERSC). Periodic boundary conditions were applied in all three directions. Afterward, the entire system was minimized for 20,000 steps followed by 20 or 40 ns of equilibration. A time step of 2 fs was used in all simulations. The temperature and pressure of the systems were held constant at 1 atmosphere and 310 K respectively, using the isothermal-isobaric ensemble with the Langevin piston and Hoover method, as successfully used for modeling integrins (20–22). We performed 20 or 40 ns of MD simulation for each run, and the trajectories were used for all analyses. The cutoff distance for non-bonded interactions was 1.2 nm, and the particle mesh Ewald method was used for electrostatic force calculations (15). All B-factors were set at zero. The hydrogen atom bond length was constrained using the SHAKE algorithm (23).

Structure Analysis—Two parameters, root mean square deviation (r.m.s.d.) values of the LIMBS metal ion and the energy of interaction of the metal ion with the LIMBS pocket, were used to evaluate stability of the metal ion at LIMBS. The r.m.s.d. of a single atom is a measure of its distance at each time step from the initial position of the ion. Hence, higher r.m.s.d. values represent fluctuations with larger amplitudes and less stable ion pocket bonds. Higher interaction energies reflect higher bond stability between the ion and LIMBS or between the α-subunit and the LIMBS loop comprising residues Arg^{216}, Asp^{217}, and Ala^{218}. To let systems equilibrate for a considerable time span before starting to take samples for r.m.s.d. measurements, r.m.s.d. values for the ion were averaged over time steps between $t = 16$–20 ns for all simulations ($n = 40$). Energies of interaction between the divalent ion and the LIMBS pocket were estimated using Langevin dynamics. As this energy of interaction did not show significant fluctuations throughout the simulations, values for energy were averaged over $t = 0$–20 ns ($n = 200$).

Reagents and Site-directed Mutagenesis—Restriction and modification enzymes were obtained from New England Biolabs Inc. (Beverly, MA), Invitrogen Life Technologies, or Fisher Scientific. All cell culture reagents were obtained from Invitrogen Life Technologies. The non-inhibitory monoclonal antibody (mAb) AP3 (American Type Culture Collection, ATCC) detects the β_3 subunit in all conformations. The heterodimer-

specific mouse mAbs CD41P2 to $\alpha_{IIb}\beta_3$ and LM609 to $\alpha_V\beta_3$ were from Millipore (Danvers, MA). The function-blocking anti-β_1 mAb P5D2 was from R&D Systems, Inc. (Minneapolis, MN). Mouse mAb AP5 detects the N-terminal sequence in the PSI domain only in high affinity/ligand-bound states. The Fab fragment of AP5 was prepared by papain digestion followed by anion exchange and size-exclusion chromatography. The allophycocyanin-labeled goat anti-mouse Fc-specific IgG antibody was from Jackson ImmunoResearch Laboratories (West Grove, PA). Recombinant $\alpha_V\beta_3$-specific high affinity fibronectin 10 domain (hFN10) (24) was expressed and purified from *Escherichia coli* as described (25), and fibronectin-depleted human fibrinogen (FB) was obtained from Enzyme Research Laboratories (South Bend, IN,). Wild-type ligands FN10 and FB and mAbs AP5 (Fab) and AP3 (IgG) were labeled respectively with *N*-hydroxy succinimidyl esters of Fluor 488 (Alexa Fluor 488) or Alexa Fluor 647 (Invitrogen) according to the manufacturer's instructions. Excess dye was removed using Centri-Spin size-exclusion microcentrifuge columns (Princeton Separations, Adelphia, NJ). The final hFN10, FB, AP5, and AP3 concentrations and dye-to-protein molar ratios (F/P) were determined spectrophotometrically, giving dye:protein molar ratios of 1–5. F191/W (F/W) and F992F/A992A (FF/AA) substitutions in human α_{IIb}, W179/F (W/F), and F990F/A990A (FF/AA) substitutions in human α_V and β-genu deletion (Δ-genu) or D158/N (D/N) substitutions in β_3 (26) were introduced using site-directed mutagenesis with the QuikChange kit (Agilent Technologies) and confirmed by DNA sequencing.

Transfections and mAb Binding—HEK293T (ATCC) cells were transiently co-transfected with pcDNA3 plasmids encoding different combinations of wild type and mutant β_3 integrins using Lipofectamine 2000 reagent (Invitrogen) according to the manufacturer's protocol. Plasmids used encoded full-length wild-type $\alpha_{IIb}\beta_3$ or $\alpha_V\beta_3$, the respective integrin carrying F191/W ($\alpha_{IIb}{}^{F/W}\beta_3$) or W179/F ($\alpha_V{}^{W/F}\beta_3$) substitutions or encoding constitutively active forms of these integrins by substituting the conserved transmembrane motif F992F (in α_{IIb}) or F990F (in α_V) to AA (27) (yielding $\alpha_{IIb}{}^{F/W+FF/AA}\beta_3$ and $\alpha_V{}^{W/F+FF/AA}\beta_3$, respectively) or by deleting the β-genu (Δ-genu) sequence (E^{476}DYRPSQ) in β_3 (26) (yielding $\alpha_{IIb}\beta_3{}^{\Delta\text{-genu}}$ and $\alpha_{IIb}{}^{F/W}\beta_3{}^{\Delta\text{-genu}}$). In addition, two mutations were created in constitutively active $\alpha_{IIb}\beta_3$, one known to cause loss of binding to FB (Y189/A, Y/A in α_{IIb}) (28) ($\alpha_{IIb}{}^{Y/A}\beta_3{}^{\Delta\text{-genu}}$), and the second by substituting the LIMBS metal-coordinating residue Asp^{158} with asparagine ($\alpha_{IIb}{}^{FF/AA}\beta_3{}^{D/N}$). 48 h after transfection, cells were detached (10 mM EDTA/PBS) and washed twice in Hanks' balanced saline solution (HBSS) and once in HBSS containing 1 mM $CaCl_2$/1 mM $MgCl_2$ ($HBSS^{2+}$). 6×10^5 $\alpha_{IIb}\beta_3$-expressing cells in 100 μl of HBSS+0.5% BSA were stained with the Alexa Fluor 647-labeled Fab fragment of AP5 (10 μg/ml; 30 min; room temperature) followed by one wash and then fixed (1% buffered paraformaldehyde). To assess β_3 integrin expression levels, 6×10^5 cells in 100 μl of HBSS+0.5% BSA were incubated with CD41-P2 (anti-$\alpha_{IIb}\beta_3$) mAb or LM609 (anti-$\alpha_V\beta_3$) mAb at 10 μg/ml for 30 min at 4 °C followed by one wash and then addition of allophycocyanin-labeled anti-mouse Fc-specific IgG (10 μg/ml) for 20 min on ice. Samples were again washed once in HBSS and then fixed. Other cells were labeled with Alexa Fluor 647-labeled AP3 (anti-β_3) (at 10 μg/ml; 30 min; 4 °C), washed once in HBSS, and then fixed. 20,000 cells were analyzed for each sample using a FACSCalibur or LSR-Fortessa flow cytometer (BD Biosciences). Binding of CD41-P2, LM609, AP3, and AP5 to β_3 integrin-expressing HEK293T was expressed as mean fluorescence intensity, as determined using the FlowJo software (BD Biosciences). Cell binding of AP5 was normalized by dividing its mean fluorescence intensity by the mean fluorescence intensity for CD41-P2 and multiplying by 100.

Soluble Ligand Binding Assays—For ligand binding experiments, 1 mM $CaCl_2$/1 mM $MgCl_2$ or 1 mM $MnCl_2$ was added to 6×10^5 β_3 integrin-expressing HEK293T cells in 100 μl of HBSS buffer containing 0.5% BSA and incubated in the presence of a saturating amount of Alexa Fluor 488-labeled FB (160 μg/ml) or Alexa Fluor 488-labeled wild-type FN10 (12.6 μg/ml) for 30 min at 25 °C. To block any potential interaction of FN10 with endogenous β_1 integrins in HEK293T, $\alpha_{IIb}\beta_3$-expressing HEK293T cells were preincubated with the function-blocking anti-β_1 mAb P5D2 before adding Alexa Fluor 488-labeled FN10. Saturating amounts of each ligand were derived from dose-response curves, where labeled ligand was added in increasing concentrations to HEK293T cells expressing constitutively active β_3 integrins in the presence of 1 mM $MnCl_2$. Integrin-ligand interactions in the presence of varying concentrations of Mn^{2+} were measured by adding increasing amounts of $MnCl_2$ to a mixture of β_3 integrin-expressing cells and saturating amounts of Alexa Fluor 488-labeled ligand. Treated cells were then incubated with Alexa Fluor 647-labeled AP3 (10 μg/ml; 30 min; 4 °C) followed by washing once in HBSS containing the corresponding concentration of Mn^{2+}. Cells were then fixed with 1% paraformaldehyde and analyzed by flow cytometry. Binding of soluble ligand to β_3 integrin-expressing cells was normalized by dividing mean fluorescence intensity by that for Alexa Fluor 647-labeled AP3 and multiplying by 100. Mean and S.D. values from three independent experiments were calculated and compared using Student's *t* test. Non-linear curve fittings of the dose-response curves were performed using GraphPad Prism (GraphPad Software Inc., La Jolla, CA).

RESULTS

LIMBS Structure and Stability of the Metal Ion in β_3 Integrins—Measurements of the energy of interaction of α_V and α_{IIb} subunits with the α-subunit-facing LIMBS loop residues Arg^{216}-Asp^{217}-Ala^{218} revealed a stronger (2–3-fold) interaction of α_V with the LIMBS loop when compared with α_{IIb}. This difference was first detected at 8 ns of simulations and maintained through 40 ns (Fig. 2*A*).

MD simulations after a few nanoseconds of equilibration showed that Ca^{2+} coordination at LIMBS in $\alpha_{IIb}\beta_3$ comprised six "primary" oxygens (*i.e.* the two carboxyl oxygens of Asp^{158} and Asp^{217}, one carboxyl oxygen of Glu^{220}, and the carbonyl oxygen of Pro^{219}) (Fig. 2*B*), which hold a mean distance of 2.2–2.3 Å from the encapsulated cation for the entire simulation, along with two "secondary" oxygens (*i.e.* the carbonyl oxygens of Asp^{217} and Ala^{218}), whose mean distance from the cation was no more than 4.5 Å over the whole trajectory. The primary oxygens remained in close contact with the Ca^{2+} at LIMBS,

forming highly stable bonds with a mean length of 2.2–2.3 Å and fluctuation amplitude below 0.5 Å. The primary coordinating oxygens formed an octahedral arrangement, with a planar surface formed by OD2 of Asp^{158}, OE1 of Glu^{220}, OD1 of Asp^{217}, and the carbonyl oxygen of Pro^{219}, with OD1 of Asp^{158} and OD2 of Asp^{217} at the top and bottom of the plane, respectively (Fig. 2*B*), restricting cation fluctuations. Replacing Ca^{2+} with Mn^{2+} in LIMBS, MIDAS, and ADMIDAS of $\alpha_{IIb}\beta_3$ increased the energy of interaction of Mn^{2+} with LIMBS by 5–8% and had a small but significant effect on r.m.s.d. (Table 1).

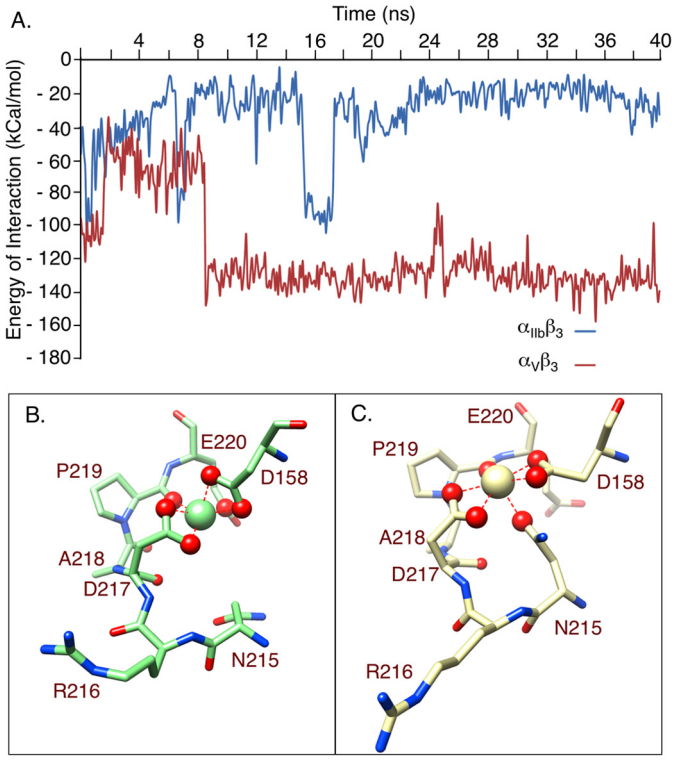

FIGURE 2. **α-subunit/LIMBS interaction energies and LIMBS conformations in β_3 integrins.** *A*, computed energy of interaction between α_{IIb} and α_V subunits and LIMBS loop residues Arg^{216}-Ala^{218}. The two trajectories appear to equilibrate after around 8 ns of simulation. The transient peak seen afterward (at ~16 ns) most likely represents a high energy local minimum state that the system occasionally takes, rather than simply a random fluctuation. *B* and C, snapshots of molecular dynamics simulations at $t = 20$ ns, showing structures of LIMBS in $\alpha_{IIb}\beta_3$ (*B*) and $\alpha_V\beta_3$ (*C*), in the same orientation, with the LIMBS Ca^{2+} shown as a *large sphere* in each case. In $\alpha_{IIb}\beta_3$, the LIMBS metal ion contacts six primary oxygens (*magnified red spheres*) and two secondary oxygens (*small red spheres*) (*B*). In $\alpha_V\beta_3$, the LIMBS metal ion also contacts six primary oxygens but only one secondary oxygen (*C*). Note that the side chain of Arg^{216} is stretched out in *C versus* in *B* and that five primary oxygens in $\alpha_V\beta_3$ (*C*) lie in one plane, in contrast to the octahedral arrangement of the primary oxygens in $\alpha_{IIb}\beta_3$ (*B*).

In contrast, the LIMBS pocket is distorted toward a planar shape in $\alpha_V\beta_3$ (Fig. 2*C*), the result of the stronger interaction that pulled the LIMBS loop toward α_V, changing metal ion coordination at this site. MD simulations showed that Ca^{2+} at LIMBS is coordinated by six primary oxygens (the two carboxyl oxygens of Asp^{158} and Asp^{217}, the carbonyl oxygen of Pro^{219}, and the carboxyl oxygen of Asn^{215}), but only one secondary coordinating oxygen, the carbonyl oxygen from Asp^{217} (Fig. 2*C*). The carboxyl oxygens of Asp^{158} and Asp^{217} as well as the carbonyl oxygen of Pro^{219} all form one planar surface that surrounds the cation, with only the side chain oxygen of Asn^{215} interacting with the cation at the bottom of the plane (Fig. 2*C*). These changes made Ca^{2+} at LIMBS significantly less stable in $\alpha_V\beta_3$ when compared with $\alpha_{IIb}\beta_3$, as reflected by the significantly higher r.m.s.d. and lower energy of interaction of the metal with LIMBS (Table 1). Replacing Ca^{2+} with Mn^{2+} in LIMBS, MIDAS, and ADMIDAS of $\alpha_V\beta_3$ had minimal effects on r.m.s.d. or on the energy of interaction of Mn^{2+} with LIMBS (Table 1).

Structural Basis for the Stronger Interaction of α_V with the LIMBS Loop—In $\alpha_V\beta_3$, all three LIMBS loop residues were involved in more extensive interactions with α_V: Arg^{216} side chain was engaged in strong ionic bonds with Glu^{121} and Glu^{123}, and its carbonyl oxygen occasionally H-bonded the side chain of Tyr^{178} (H-bond probability 0.5%). Arg^{216} also formed van der Waals contacts with Phe^{154} and with the indole group of Trp^{179} (Fig. 3, *A* and *B*). In addition, the main and side chains of Asp^{217} formed van der Waals contacts with the indole group of Trp^{179}, and the side chain of Ala^{218} contacted the carboxyl oxygen of Asp^{219} in α_V. These interactions stretched the LIMBS loop toward α_V, distorting LIMBS.

In contrast, interaction of α_{IIb} with LIMBS loop residues Arg^{216}-Asp^{217}-Ala^{218} was primarily limited to Arg^{216}. The side chain of Arg^{216} formed intermittent H-bonds with the hydroxyl group of Tyr^{190} (H-bond probability 5.0%), and its carbonyl oxygen contacted the side chain of Tyr^{190} (Fig. 3*C*). Arg^{216} side chain also formed occasional ionic interactions with Glu^{123} (Fig. 3*D*), but made no contacts with Phe^{191}. Additionally, Asp^{232} made intermittent van der Waals contacts with the side chain of Ala^{218}.

TABLE 1
Summary of mean r.m.s.d. and interaction energy values for tested β_3 integrins

Integrin and β_3 metal ion occupancy state	$\alpha_{IIb}\beta_3$ (Ca^{2+}-Mg^{2+}-Ca^{2+})			$\alpha_{IIb}\beta_3$ (Mn^{2+}-Mn^{2+}-Mn^{2+})[a]			$\alpha_V\beta_3$ (Ca^{2+}-Mg^{2+}-Ca^{2+})[a]		$\alpha_V\beta_3$ (Mn^{2+}-Mn^{2+}-Mn^{2+})[a]	
	Wild type	F191/W	D158/N	Wild type	F191/W	D158/N	Wild type	W179/F	Wild type	W179/F
r.m.s.d. (Å)										
Mean	2.0	8.3	14.5	2.7	11.8	4.7	12.3	6.1	11.0	4.7
S.D.	0.5	1.2	1.2	1.4	1.1	1.1	0.7	0.7	0.8	1.0
p value[b]		<0.001	<0.001	0.002	<0.001	<0.001	<0.001	<0.001	<0.001	<0.001
Energy of interaction between LIMBS and metal ion (kcal/mol)										
Mean	859	865	620	930	913	752	775	732	779	780
S.D.	20	14	14	17	23	15	15	13	15	16
p value[b]		<0.001	<0.001	<0.001	<0.001	<0.001	<0.001	<0.001	<0.001	<0.001

[a] Integrin mutation.
[b] All *p* values were compared to wild-type $\alpha_{IIb}\beta_3$ (Ca^{2+}-Mg^{2+}-Ca^{2+}) structure.

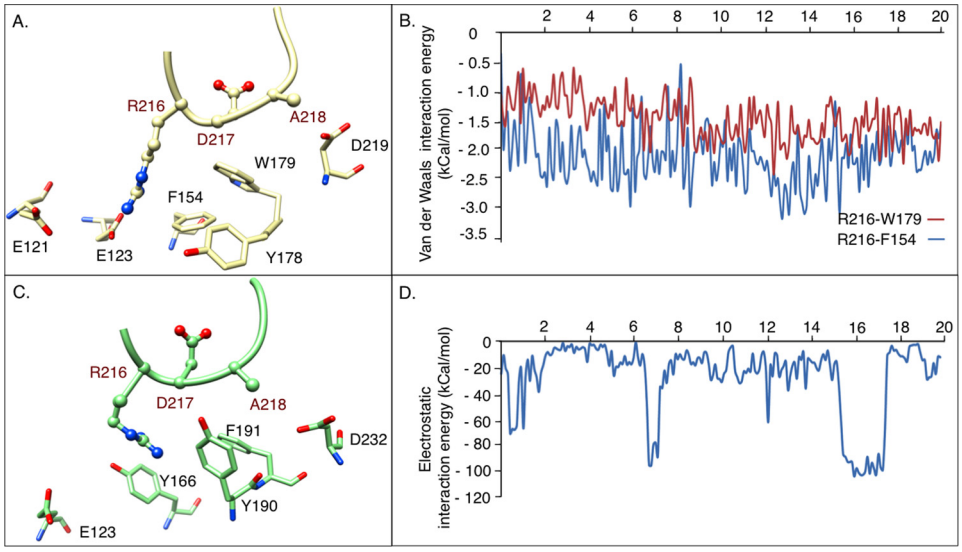

FIGURE 3. **α-subunit residues interacting with the LIMBS loop.** *A*, snapshot of MD simulations at 20 ns showing interactions of the LIMBS loop Arg^{216}-Ala^{218} residues (shown as *ball and stick*) with α_V subunit residues (shown as *stick*). The structures in *A* and *C* are shown in the same orientation after superposing LIMBS of each. LIMBS residues are labeled *red* in *A* and *C* (also in Figs. 4*B* and 5*B*). In α_V, the LIMBS loop interacts with the Phe^{154}, Tyr^{178}, Trp^{179}, Asp^{219}, Glu^{121}, and Glu^{123} of α_V. *B*, MD simulations showing van der Waals energy of interaction between Arg^{216} of the LIMBS loop with Trp^{179} and Phe^{154} of α_V. *C*, snapshot of MD simulations at 20 ns showing interactions of the LIMBS loop Arg^{216}-Ala^{218} residues with α_{IIb} subunit residues (shown as *stick*). In α_{IIb}, interactions are limited to the corresponding residues Tyr^{166}, Tyr^{190}, Phe^{191}, and Asp^{232} and a transient interaction with Glu^{123}. *D*, electrostatic energy of interaction between Arg^{216} of the LIMBS loop and Glu^{123} of α_{IIb}. Occasional jumps to higher energy levels represent ionic bonds between Arg^{216} and Glu^{123}. The energy peaks at $t = 7$ and 16 ns show sharp increases to the same value of about 100 kcal/mol, suggesting that the ionic bond occurs at a local energy minimum that the system continues to take, whereas the Arg^{216}-Glu^{123} bond spends most of the simulation time in a lower electrostatic energy state (*i.e.* longer bond distance).

Effects of Modifying α_{IIb} and α_v on Stability of the Metal Ion at LIMBS—Of the α-subunit residues contacting the LIMBS loop residues Arg^{216}-Asp^{217}-Ala^{218}, the side chains of Phe^{191} in α_{IIb} and Trp^{179} in α_V are superimposable (Fig. 1). We evaluated the impact of interchanging these two residues on stability of the metal ion at LIMBS in the two β_3 integrins. As an internal control, we measured the effects of destabilizing the metal ion at LIMBS through the D158/N substitution (which removes one of the main coordinating oxygens from the metal ion). MD simulations showed that implementing the D158/N mutation in $\alpha_{IIb}\beta_3$ yielded a significant increase in r.m.s.d. (~2-fold) and a reduction in the energy of interaction (Table 1), both reflecting destabilization of the metal ion at LIMBS.

Implementing the F191/W substitution in α_{IIb} significantly increased the energy of interaction of the LIMBS loop with the bulkier Trp^{191} in $\alpha_{IIb}^{F/W}$ when compared with Phe^{191} in wild-type α_{IIb} (Fig. 4*A*). Snapshot of the structure at $t = 20$ ns showed that the side chain of Arg^{216} of β_3 releases its interaction with Tyr^{190} and forms van der Waals contacts with the indole group of Trp^{191} in $\alpha_{IIb}^{F/W}$ (compare Fig. 4*B* with Fig. 3*C*), pulling the LIMBS loop region toward the $\alpha_{IIb}^{F/W}$ propeller domain. With Trp^{191} and Tyr^{190} pulling the LIMBS loop in the same direction, Ala^{218} is brought closer to Asp^{232} to form more contacts, increasing the energy of interaction of $\alpha_{IIb}^{F/W}$ with the LIMBS loop and deforming the octahedral shape of the pocket. These movements displaced the oxygens forming the LIMBS pocket from their native pattern toward a more planar configuration. Although the energy of interaction of Ca^{2+} or Mn^{2+} with the LIMBS pocket in the $\alpha_{IIb}^{F/W}\beta_3$ structure did not change, r.m.s.d. increased by ~4-fold (Table 1). Hence, it appears that the energetic component of the free energy remains unchanged upon applying

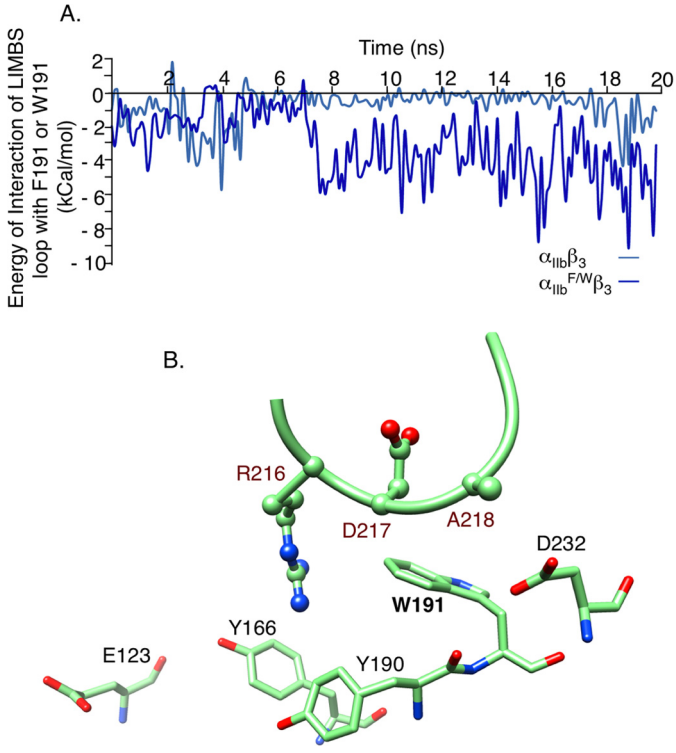

FIGURE 4. **Effect of F191/W change in $\alpha_{IIb}\beta_3$ on interaction energies and shape of LIMBS.** *A*, computed energy of interaction between LIMBS loop residues Arg^{216}-Ala^{218} and Trp^{191} in $\alpha_{IIb}^{F/W}$. *B*, snapshot at $t = 20$ ns of the interactions of LIMBS loop with $\alpha_{IIb}^{F/W}$ residues Tyr^{166}, Tyr^{190}, Trp^{191}, Asp^{232}, and Glu^{123}. Mutating Phe^{191} to Trp in $\alpha_{IIb}^{F/W}$ enhanced interactions of the larger Trp^{191} side chain with the LIMBS loop, especially with Arg^{216}, modifying the conformation of the LIMBS pocket (see "Results").

F191/W, whereas the entropic component is highly changed upon deformation of the pocket as represented by a 4-fold increase in r.m.s.d.

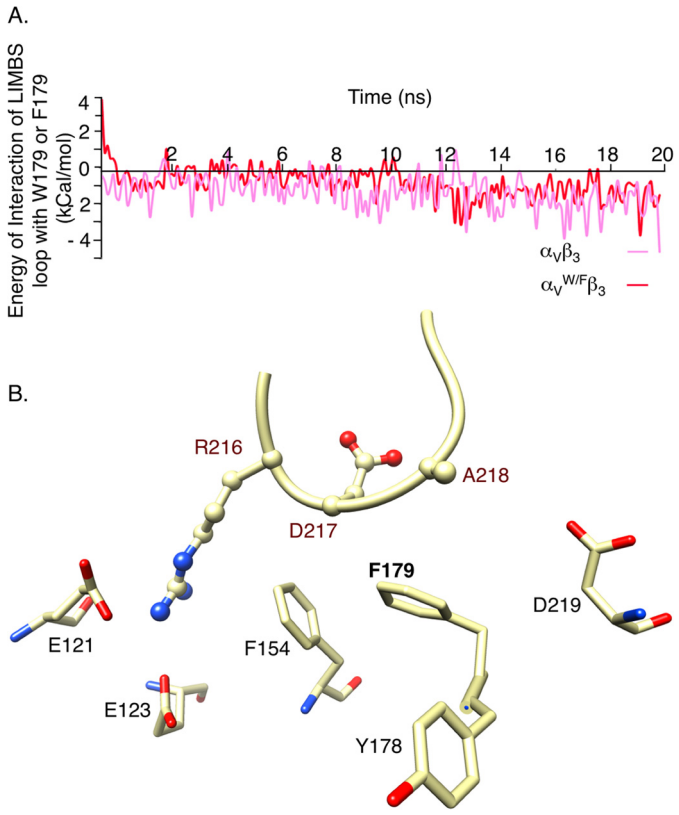

FIGURE 5. **Effect of W179/F in $\alpha_V\beta_3$ on interaction energies and shape of LIMBS.** *A*, computed energy of interaction between the LIMBS loop residues Arg^{216}-Ala^{218} and Phe^{179} in $\alpha_V^{W/F}$. Mutating Trp^{179} to Phe does not change the energy of interaction with the LIMBS loop significantly. *B*, snapshot at t = 20 ns of interactions of the LIMBS loop with α_V subunit residues Glu^{121}, Glu^{123}, Phe^{154}, Phe^{179}, and Asp^{219}. The W179/F mutation weakens interaction of LIMBS loop with $\alpha_V^{W/F}$, reshaping the LIMBS pocket. The structure is shown in the same orientation as in Fig. 4*B*.

Implementing the W179/F substitution in $\alpha_V^{W/F}$ did not change the energy of interaction of the LIMBS loop with $\alpha_V^{W/F}$ (Fig. 5*A*). However, it reduced fluctuations of the Ca^{2+} or Mn^{2+} at LIMBS (r.m.s.d. reduced by ~2-fold, Table 1), the result of removing the contacts between Trp^{179} and the LIMBS loop (Fig. 5*B*). The W179/F substitution did not significantly change the interaction energy of the metal ion with LIMBS (Table 1) because it did not affect the other interactions of α_V with the LIMBS loop, particularly with Arg^{216} (Fig. 5*B*).

Binding of Wild-type and F191/W Mutant $\alpha_{IIb}\beta_3$ to Soluble Ligand—We next sought experimental validation of the computational studies. We expressed recombinant $\alpha_{IIb}^{F/W}\beta_3$ in its resting and mutationally activated ($\alpha_{IIb}^{F/W+FF/AA}\beta_3$, $\alpha_{IIb}^{F/W}\beta_3^{\Delta\text{-genu}}$) states in HEK293T cells and compared its surface expression, structure, and ligand binding capacity with that of constitutively active wild type $\alpha_{IIb}^{FF/AA}\beta_3$. As shown in Fig. 6*A*, surface expression of the mutant resting or constitutively active heterodimeric receptor was comparable with that of resting or constitutively active wild-type $\alpha_{IIb}\beta_3$, and the F191/W mutation did not change the recognition of the constitutively active integrin by the ligand-induced binding site (LIBS) mAb AP5 (Fig. 6*B*). Binding of WT $\alpha_{IIb}\beta_3$ to soluble Alexa Fluor 488-labeled FB (Alexa Fluor 488-FB) was minimal in the presence of 1 mM each of the physiologic divalent cations Ca^{2+} and Mg^{2+} (Ca^{2+}/Mg^{2+}), but increased only slightly in 1 mM Mn^{2+} (Fig. 6*C*). $\alpha_{IIb}^{F/W+FF/AA}\beta_3$,

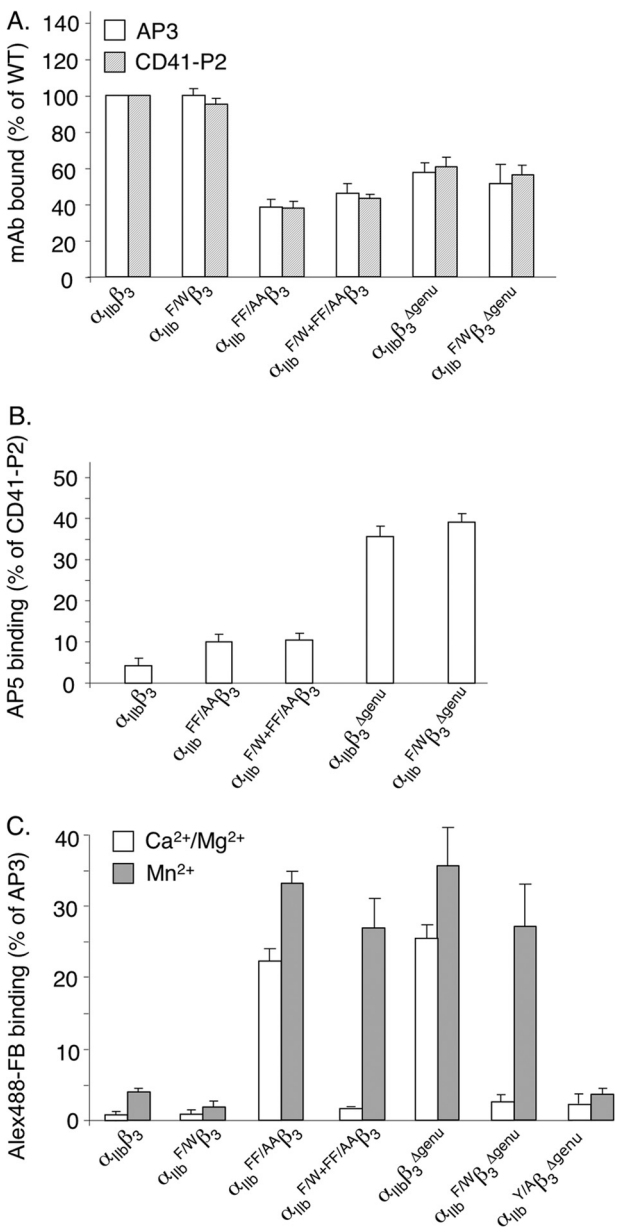

FIGURE 6. **Effect of α_{IIb} F191/W mutation in $\alpha_{IIb}\beta_3$ on cell surface expression, activation, and binding to soluble ligand.** *A*, histograms (mean ± S.D.; n = 3) comparing cell surface expression and heterodimer formation of $\alpha_{IIb}\beta_3$, $\alpha_{IIb}^{F/W}\beta_3$, and constitutively active $\alpha_{IIb}^{FF/AA}\beta_3$, $\alpha_{IIb}\beta_3^{\Delta\text{-genu}}$, $\alpha_{IIb}^{F/W+FF/AA}\beta_3$, and $\alpha_{IIb}^{F/W}\beta_3^{\Delta\text{-genu}}$. Constitutive activation reduced expression of the wild type and F191/W integrin to equivalent degrees. *B*, histograms (mean ± S.D.; n = 3) showing binding of the LIBS mAb AP5 to $\alpha_{IIb}\beta_3$ and to constitutively active $\alpha_{IIb}^{FF/AA}\beta_3$, $\alpha_{IIb}^{F/W+FF/AA}\beta_3$, $\alpha_{IIb}\beta_3^{\Delta\text{-genu}}$, and $\alpha_{IIb}^{F/W}\beta_3^{\Delta\text{-genu}}$. Binding was expressed as a percentage of binding of the heterodimer-specific mAb CD41-P2. *C*, histograms (mean ± S.D.; n = 3) showing binding of wild-type and constitutively active $\alpha_{IIb}^{F/W+FF/AA}\beta_3$ to saturating amounts of soluble Alexa Fluor 488-FB (*Alex488-FB*) in 1 mM Ca^{2+} plus 1 mM Mg^{2+} (Ca^{2+}/Mg^{2+}) or 1 mM Mn^{2+}. Binding is expressed as a percentage of Alexa Fluor 647-AP3 mAb staining. F191/W did not significantly impair ligand binding to constitutively active $\alpha_{IIb}\beta_3$ in Mn^{2+}. However, ligand binding to constitutively active $\alpha_{IIb}\beta_3$ in Mn^{2+} was abolished when the ligand contact residue Tyr^{189} was simultaneously mutated to Ala.

$\alpha_{IIb}^{F/W}\beta_3^{\Delta\text{-genu}}$ bound constitutively to Alexa Fluor 488-FB in Ca^{2+}/Mg^{2+}-containing buffer, as expected, with 1 mM Mn^{2+} further increasing ligand binding by ~1.5-fold (Fig. 6*C*).

Cellular $\alpha_{IIb}^{F/W}\beta_3$ showed minimal binding to soluble Alexa Fluor 488-FB in Ca^{2+}/Mg^2 buffer, with 1 mM Mn^{2+} increasing binding by ~2-fold (Fig. 6*C*). Introduction of the F191/W muta-

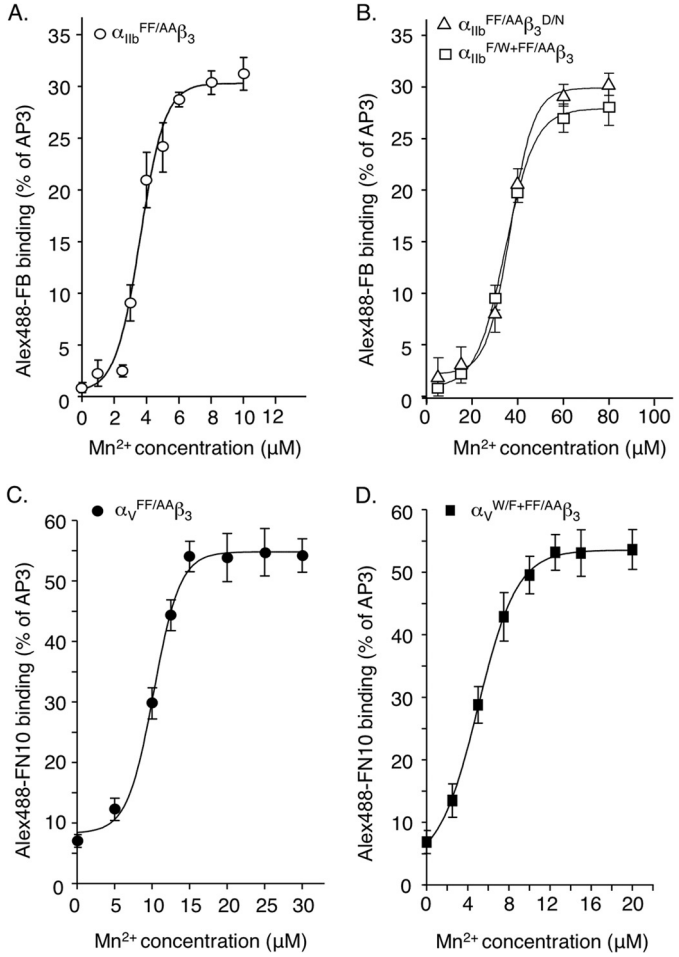

FIGURE 7. **Effect of $\alpha_{IIb}^{F/W}$, $\alpha_V^{W/F}$, and $\beta_3^{D/N}$ mutations on integrin-ligand interactions in the presence of varying concentrations of Mn^{2+}.** *A* and *B*, dose-response curves comparing binding of $\alpha_{IIb}^{FF/AA}\beta_3$ (*A*) and $\alpha_{IIb}^{FF/AA}\beta_3^{D/N}$ and $\alpha_{IIb}^{F/W+FF/AA}\beta_3$ (*B*) with saturating amounts of soluble Alexa Fluor 488-FB (*Alex488-FB*) in the presence of increasing concentrations of Mn^{2+}. *C* and *D*, dose-response curves comparing binding of cellular $\alpha_V^{FF/AA}\beta_3$ (*C*) and $\alpha_V^{W/F+FF/AA}\beta_3$ (*D*) with saturating amounts of soluble Alexa Fluor 488-FN10 in the presence of increasing concentrations of Mn^{2+}. Binding was expressed as a percentage of Alexa Fluor 647-AP3 mAb binding.

tion in constitutively active $\alpha_{IIb}^{F/W+FF/AA}\beta_3$ and $\alpha_{IIb}^{F/W}\beta_3^{\Delta\text{-genu}}$ integrins abolished ligand binding in the presence of Ca^{2+}/Mg^{2+}, but did not reduce binding in the presence of 1 mM Mn^{2+} (Fig. 6*C*). As a negative control, replacing the ligand contact residue Tyr^{189} in α_{IIb} with alanine abolished binding of cellular $\alpha_{IIb}^{YA}\beta_3^{\Delta\text{-genu}}$ to soluble Alexa Fluor 488-FB in 1 mM Mn^{2+} (Fig. 6*C*), in agreement with a published study (28).

Effects of F191/W in α_{IIb} and W179/F in α_V on Apparent Affinity of Mn^{2+} to the Respective Integrins—We measured the binding of constitutively active wild-type and mutant β_3 integrins to saturating amount of soluble ligand across a range of Mn^{2+} concentrations. Half-maximal binding of $\alpha_{IIb}^{FF/AA}\beta_3$ to Alexa Fluor 488-FB was achieved at an Mn^{2+} concentration of 5.9 μM ± 2.1 (mean ± S.D., $n = 3$) (Fig. 7*A*). Removing one of the LIMBS metal-coordinating oxygens (through the D158/N mutation) increased the Mn^{2+} concentration required for half-maximal binding of ligand to $\alpha_{IIb}^{FF/AA}\beta_3^{D/N}$ by ~6-fold to 36.7 ± 8.6 μM, an indirect measure of the reduction in apparent affinity ($K_{d(app)}$) of Mn^{2+} to $\alpha_{IIb}^{FF/AA}\beta_3^{D/N}$ (Fig. 7*B*). The F191/W substitution in $\alpha_{IIb}^{FF/AA}\beta_3$ yielded an almost identical value (34.6 ± 6.2 μM) (Fig. 7*B*). In contrast, the W179/F mutation in α_V significantly increased the apparent $K_{d(app)}$ of Mn^{2+} to the $\alpha_V^{W/F+FF/AA}\beta_3$ heterodimer (as judged by mAb LM609 binding, not shown) by ~2-fold (mean ± S.D., 5.0 ± 1.9 μM from 10.2 ± 3.5 μM to $\alpha_V^{FF/AA}\beta_3$, $p = 0.018$) (Fig. 7, *C* and *D*).

DISCUSSION

In this study, we provide computational and functional evidence that the α-subunit plays an essential role in stability of the metal ion coordination at LIMBS in β_3 integrins. By combining these two approaches, we demonstrated the following. 1) interaction of the LIMBS loop with α_V is more extensive than with α_{IIb}; 2) metal ion coordination at LIMBS after 20 ns of equilibration becomes planar in $\alpha_V\beta_3$; 3) changing the α_{IIb}-LIMBS loop interface residue Phe^{191} to Trp destabilized the metal ion at LIMBS, whereas a Trp^{179} to Phe mutation in α_V produced opposite but weaker effects; and 4) introducing F191/W in cellular $\alpha_{IIb}\beta_3$ reduced the apparent affinity of Mn^{2+} to this integrin; the reverse was observed upon introducing the W179/F mutation in cellular $\alpha_V\beta_3$.

The higher energy of interaction of α_V with the LIMBS loop residues Arg^{216}-Ala^{218} was directly related to the more extensive contacts α_V made with this loop when compared with α_{IIb}. The stronger contacts increased fluctuations of the metal ion at LIMBS in $\alpha_V\beta_3$, as reflected by the ~4-fold increase in r.m.s.d., and also increased the mean distances between the coordinating oxygens and the metal ion at LIMBS, as reflected by the reduction in total energy of interaction of the metal ion with the pocket. These observations may offer an explanation for the variable occupancy of LIMBS by metal ion in crystal structures of unliganded $\alpha_V\beta_3$ ectodomains, where LIMBS was metal-occupied in one (4g1e.pdb, used in this study) (13) but not in four other unliganded $\alpha_V\beta_3$ ectodomain structures (9, 26, 29, 30). The lack of metal occupancy at LIMBS was attributed to unfavorable crystallization conditions (13). However, LIMBS is metal ion occupied in $\alpha_V\beta_3$ under the same crystallization conditions when $\alpha_V\beta_3$ is ligand-bound (9, 25). The data produced in this study suggest that variability in LIMBS occupancy by metal is the result of the different contacts the LIMBS loop makes with α_V in contrast to α_{IIb}. In the presence of ligand, Glu^{220} of the βA domain provides an extra primary oxygen, stabilizing the metal ion at LIMBS. In the absence of ligand, this stabilizing influence is lost, and the metal ion is freer to escape LIMBS. This scenario is reflected in the higher r.m.s.d. and lower energy of interaction of the metal ion with LIMBS in unliganded $\alpha_V\beta_3$ when compared with $\alpha_{IIb}\beta_3$ (Table 1).

$\alpha_V\beta_3$ is widely expressed in tissues including bone, where it mediates dynamic cell adhesion (31, 32). The majority of Mn^{2+} in the body is sequestered in bone (33) to levels that approach the K_d of $\alpha_V\beta_3$ for Mn^{2+} (7), suggesting that Mn^{2+} plays an important role in regulating $\alpha_V\beta_3$ function in this tissue. In contrast, $\alpha_{IIb}\beta_3$ is solely expressed on circulating platelets in blood containing high levels of its physiologic ligands, mainly fibrinogen, and mM concentrations of the divalent cations Ca^{2+} and Mg^{2+}. Maintaining $\alpha_{IIb}\beta_3$ in a dormant inactive state in this environment is therefore essential to prevent pathologic thrombosis. The present data provide insights into how regu-

lation can be tailored to the particular environment where an integrin is expressed. Occupancy of LIMBS, MIDAS, and ADMIDAS by metal ions in unliganded $\alpha_{IIb}\beta_3$ may explain the rapid ligand association rates to activated $\alpha_{IIb}\beta_3$ (7). This potential proactivation tendency at the ligand-binding site must be counteracted by energy barrier(s) to activation elsewhere to effectively keep $\alpha_{IIb}\beta_3$ in an inactive state on circulating resting platelets. One such barrier may exist in the integrin leg segments, between the α-subunit Calf-2 domain and the β_3 subunit EGF-like 4 (IE4) and βTD domains (34). Disruption of this interface rendered $\alpha_{IIb}\beta_3$ as susceptible to Mn^{2+}-induced ligand binding as $\alpha_V\beta_3$ (34). In $\alpha_V\beta_3$, where this Calf-2/IE4-βTD barrier is weak or absent (34), a relatively stronger α_V-LIMBS interface may help favor the inactive $\alpha_V\beta_3$ conformation, thus limiting stable occupancy of the metal ion in this integrin to conditions when ligand is also accessible.

Acknowledgment—We thank Dr. José Luis Alonso for helpful discussions.

REFERENCES

1. Hynes, R. O. (2002) Integrins: bidirectional, allosteric signaling machines. *Cell* **110,** 673–687
2. Arnaout, M. A., Goodman, S. L., and Xiong, J. P. (2007) Structure and mechanics of integrin-based cell adhesion. *Curr. Opin. Cell Biol.* **19,** 495–507
3. Xiong, J. P., Stehle, T., Diefenbach, B., Zhang, R., Dunker, R., Scott, D. L., Joachimiak, A., Goodman, S. L., and Arnaout, M. A. (2001) Crystal structure of the extracellular segment of integrin αVβ3. *Science* **294,** 339–345
4. Moser, M., Legate, K. R., Zent, R., and Fässler, R. (2009) The tail of integrins, talin, and kindlins. *Science* **324,** 895–899
5. Hu, D. D., Barbas, C. F., and Smith, J. W. (1996) An allosteric Ca^{2+} binding site on the β3-integrins that regulates the dissociation rate for RGD ligands. *J. Biol. Chem.* **271,** 21745–21751
6. Mould, A. P., Akiyama, S. K., and Humphries, M. J. (1995) Regulation of integrin α5β1-fibronectin interactions by divalent cations: evidence for distinct classes of binding sites for Mn^{2+}, Mg^{2+}, and Ca^{2+}. *J. Biol. Chem.* **270,** 26270–26277
7. Smith, J. W., Piotrowicz, R. S., and Mathis, D. (1994) A mechanism for divalent cation regulation of β3-integrins. *J. Biol. Chem.* **269,** 960–967
8. Loftus, J. C., O'Toole, T. E., Plow, E. F., Glass, A., Frelinger, A. L., 3rd, and Ginsberg, M. H. (1990) A β3 integrin mutation abolishes ligand binding and alters divalent cation-dependent conformation. *Science* **249,** 915–918
9. Xiong, J. P., Stehle, T., Zhang, R., Joachimiak, A., Frech, M., Goodman, S. L., and Arnaout, M. A. (2002) Crystal structure of the extracellular segment of integrin αVβ3 in complex with an Arg-Gly-Asp ligand. *Science* **296,** 151–155
10. Murcia, M., Jirouskova, M., Li, J., Coller, B. S., and Filizola, M. (2008) Functional and computational studies of the ligand-associated metal binding site of β3 integrins. *Proteins* **71,** 1779–1791
11. Valdramidou, D., Humphries, M. J., and Mould, A. P. (2008) Distinct roles of β1 metal ion-dependent adhesion site (MIDAS), adjacent to MIDAS (ADMIDAS), and ligand-associated metal-binding site (LIMBS) cation-binding sites in ligand recognition by integrin α2β1.*J. Biol. Chem.* **283,** 32704–32714
12. Zhu, J., Luo, B. H., Xiao, T., Zhang, C., Nishida, N., and Springer, T. A. (2008) Structure of a complete integrin ectodomain in a physiologic resting state and activation and deactivation by applied forces. *Mol. Cell* **32,** 849–861
13. Dong, X., Mi, L. Z., Zhu, J., Wang, W., Hu, P., Luo, B. H., and Springer, T. A. (2012) $\alpha_V\beta_3$ integrin crystal structures and their functional implications. *Biochemistry* **51,** 8814–8828
14. Guex, N., and Peitsch, M. C. (1997) SWISS-MODEL and the Swiss-PdbViewer: an environment for comparative protein modeling. *Electrophoresis* **18,** 2714–2723
15. Phillips, J. C., Braun, R., Wang, W., Gumbart, J., Tajkhorshid, E., Villa, E., Chipot, C., Skeel, R. D., Kalé, L., and Schulten, K. (2005) Scalable molecular dynamics with NAMD. *J. Comput. Chem.* **26,** 1781–1802
16. MacKerell, A. D., Jr., Banavali, N., and Foloppe, N. (2000) Development and current status of the CHARMM force field for nucleic acids. *Biopolymers* **56,** 257–265
17. Jorgensen, W. L., Chandrasekhar, J., Madura, J. D., Impey, R. W., and Klein, M. L. (1983) Comparison of simple potential functions for simulating liquid water. *J. Chem. Phys.* **79,** 926–935
18. Humphrey, W., Dalke, A., and Schulten, K. (1996) VMD: visual molecular dynamics. *J. Mol. Graph.* **14,** 33–38, 27–38
19. Pettersen, E. F., Goddard, T. D., Huang, C. C., Couch, G. S., Greenblatt, D. M., Meng, E. C., and Ferrin, T. E. (2004) UCSF Chimera: a visualization system for exploratory research and analysis. *J. Comput. Chem.* **25,** 1605–1612
20. Mehrbod, M., and Mofrad, M. R. (2013) Localized lipid packing of transmembrane domains impedes integrin clustering. *PLoS Comput. Biol.* **9,** e1002948
21. Mehrbod, M., Trisno, S., and Mofrad, M. R. (2013) On the activation of integrin αIIbβ3: outside-in and inside-out pathways. *Biophys. J.* **105,** 1304–1315
22. Chen, W., Lou, J., Hsin, J., Schulten, K., Harvey, S. C., and Zhu, C. (2011) Molecular dynamics simulations of forced unbending of integrin $\alpha_v\beta_3$. *PLoS Comput. Biol.* **7,** e1001086
23. Kräutler, V., van Gunsteren, W. F., and Hünenberger, P. H. (2001) A fast SHAKE algorithm to solve distance constraint equations for small molecules in molecular dynamics simulations. *J. Comput. Chem.* **22,** 501–508
24. Richards, J., Miller, M., Abend, J., Koide, A., Koide, S., and Dewhurst, S. (2003) Engineered fibronectin type III domain with a RGDWXE sequence binds with enhanced affinity and specificity to human αvβ3 integrin. *J. Mol. Biol.* **326,** 1475–1488
25. Van Agthoven, J. F., Xiong, J. P., Alonso, J. L., Rui, X., Adair, B. D., Goodman, S. L., and Arnaout, M. A. (2014) Structural basis for pure antagonism of integrin αVβ3 by a high-affinity form of fibronectin. *Nat. Struct. Mol. Biol.* **21,** 383–388
26. Xiong, J. P., Mahalingham, B., Alonso, J. L., Borrelli, L. A., Rui, X., Anand, S., Hyman, B. T., Rysiok, T., Müller-Pompalla, D., Goodman, S. L., and Arnaout, M. A. (2009) Crystal structure of the complete integrin αVβ3 ectodomain plus an α/β transmembrane fragment. *J. Cell Biol.* **186,** 589–600
27. Wegener, K. L., Partridge, A. W., Han, J., Pickford, A. R., Liddington, R. C., Ginsberg, M. H., and Campbell, I. D. (2007) Structural basis of integrin activation by talin. *Cell* **128,** 171–182
28. Kamata, T., Irie, A., Tokuhira, M., and Takada, Y. (1996) Critical residues of integrin αIIb subunit for binding of αIIbβ3 (glycoprotein IIb-IIIa) to fibrinogen and ligand-mimetic antibodies (PAC-1, OP-G2, and LJ-CP3). *J. Biol. Chem.* **271,** 18610–18615
29. Mahalingam, B., Van Agthoven, J. F., Xiong, J. P., Alonso, J. L., Adair, B. D., Rui, X., Anand, S., Mehrbod, M., Mofrad, M. R., Burger, C., Goodman, S. L., and Arnaout, M. A. (2014) Atomic basis for the species-specific inhibition of αV integrins by mAb 17E6 is revealed by the crystal structure of αVβ3 ectodomain-17E6 Fab complex. *J. Biol. Chem.* **289,** 13801–13809
30. Xiong, J. P., Stehle, T., Goodman, S. L., and Arnaout, M. A. (2004) A novel adaptation of the integrin PSI domain revealed from its crystal structure. *J. Biol. Chem.* **279,** 40252–40254
31. Lakkakorpi, P. T., Horton, M. A., Helfrich, M. H., Karhukorpi, E. K., and Väänänen, H. K. (1991) Vitronectin receptor has a role in bone resorption but does not mediate tight sealing zone attachment of osteoclasts to the bone surface. *J. Cell Biol.* **115,** 1179–1186
32. Roca-Cusachs, P., Gauthier, N. C., Del Rio, A., and Sheetz, M. P. (2009) Clustering of $\alpha_5\beta_1$ integrins determines adhesion strength whereas $\alpha_v\beta_3$ and talin enable mechanotransduction. *Proc. Natl. Acad. Sci. U.S.A.* **106,** 16245–16250
33. Brandt, M., and Schramm, V. L. (1986) in Manganese in Metabolism and Enzyme Function. (Schramm, V. L., and EdIer, F. C., eds), pp. 3–13, Academic Press, New York.
34. Kamata, T., Handa, M., Sato, Y., Ikeda, Y., and Aiso, S. (2005) Membrane-proximal α/β stalk interactions differentially regulate integrin activation. *J. Biol. Chem.* **280,** 24775–24783